Supplemental Figure 1.

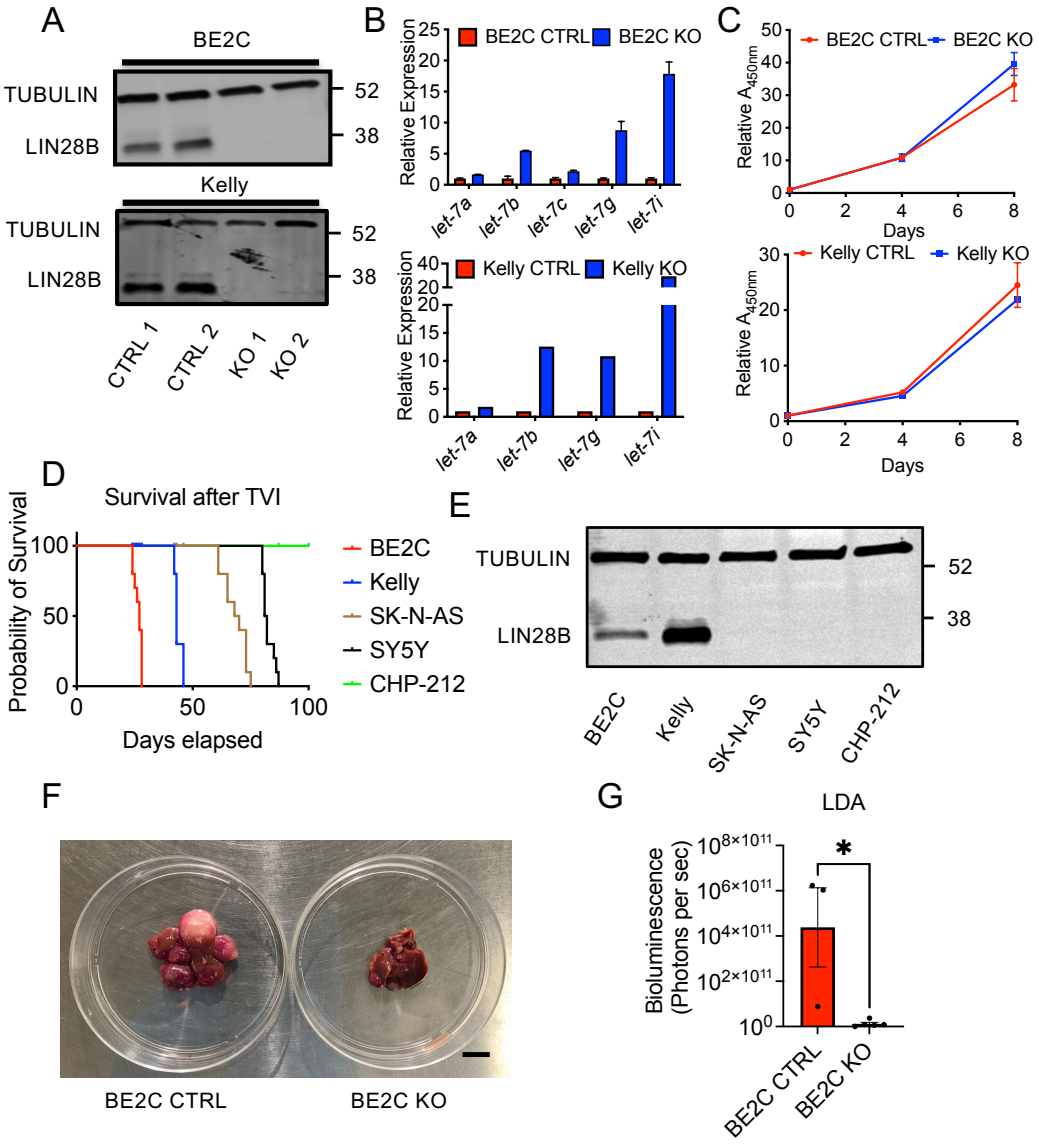

Loss of LIN28B shows profound effects in vivo compared to cell growth in vitro.

A) Western Blot of BE2C and Kelly neuroblastoma cell lines infected with V2 CRISPR/Cas9 virus to stably express Cas9 and either two non-targeting (CTRL1 and CTRL2) or *LIN28B* targeting (EX2 (KO1) and EX3.1 (KO2)) gRNAs.

B) Relative expression of different *let-7* family members of CTRL1 and KO1 cell lines.

C) Cell growth analysis of cells used in Supplemental Figures 1A/1B (using CCK-8 assay).

D) Kaplan Meier Curve for immunocompromised mice injected into tail vein with different neuroblastoma cell lines (n=10 mice/group).

E) Western Blot for LIN28B of different cell lines shown in D).

F) Representative image of tumor burden of colonized livers for the lowest dilution of mice used in Figure 1E.

G) Quantitative analysis of bioluminescence of colonized livers for the lowest dilution of mice used in Figure 1E) (n=3-5 mice/group, 2 WT reached critical tumor burden before imaging endpoint).

All statistical data were assessed using 2-tailed Student's t-test and are presented as mean±s.e.m. * = $p<0.05$. Scale bar in F) represents 1cm.

Supplemental Figure 2.

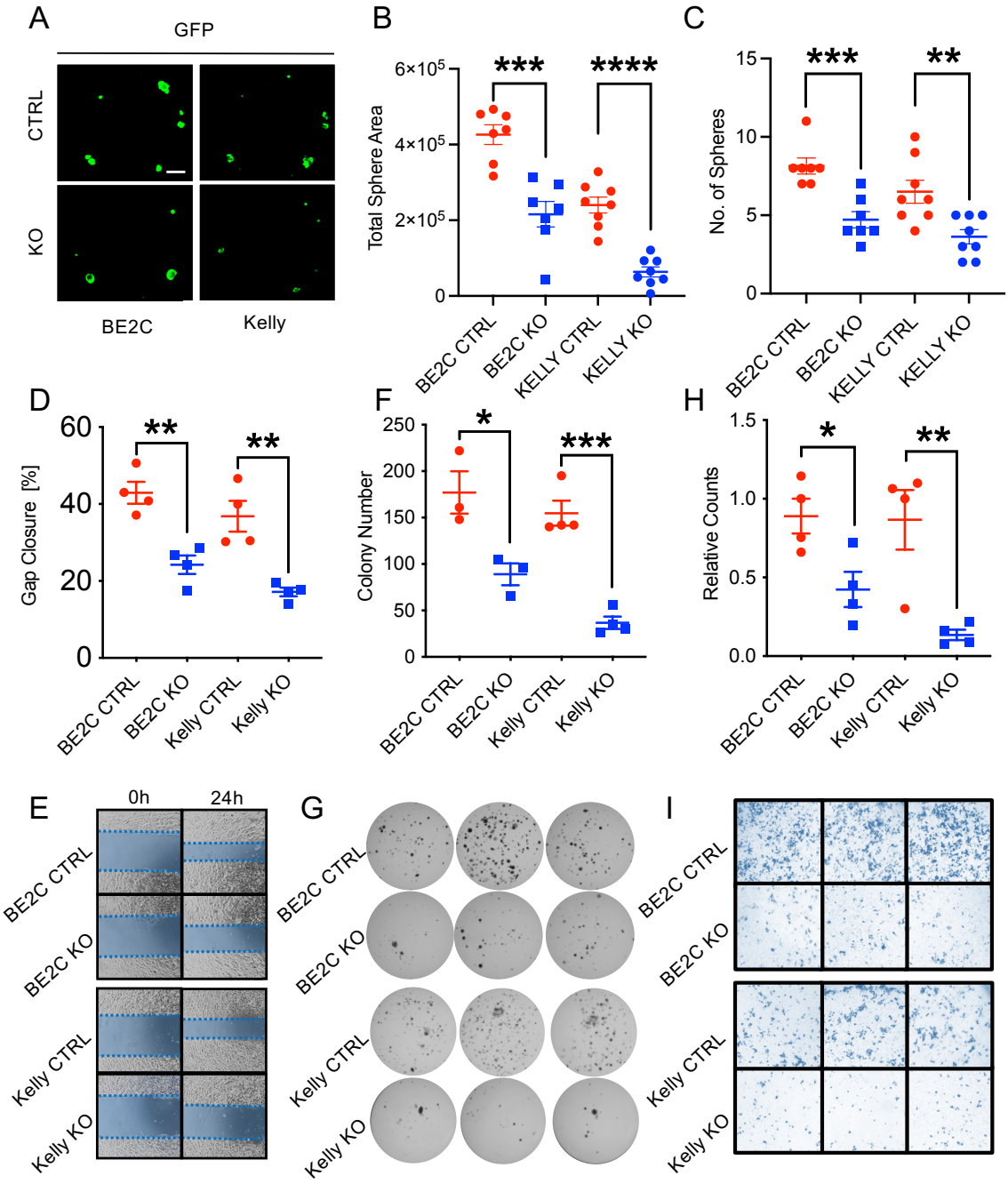

Loss of *LIN28B* expression impairs anchorage independent growth, migratory and invasive capabilities in vitro.

A) Representative fluorescence images of living tumor spheres 2 weeks after sorting of GFP expressing BE2C and Kelly cells of the indicated genotypes into low attachment plates.
B) Total sphere area of BE2C and Kelly cells assessed by ImageJ 2 weeks after sorting (n=7 (BE2C) and n=8 (Kelly) biological replicates/group).
C) Number of spheres of BE2C and Kelly cells 2 weeks after sorting (n=7 (BE2C) and n=8 (Kelly) biological replicates/group).
D) Percentage of gap closure after 24h for the indicated groups (n=4 biological replicates/group).
E) Representative pictures of wound healing assays of BE2C and Kelly cells after 0h and 24h.

F) Number of colonies 24 days after plating BE2C and Kelly cells in soft agar (n=3 (BE2C) and n=4 (Kelly) biological replicates/group).
G) Representative images of stained colonies of BE2C and Kelly cells plated in soft agar after 24 days.
H) Relative counts of migrated BE2C and Kelly cells 24h after plating (n=4 biological replicates/group).
I) Representative images of transwell migration assays of BE2C and Kelly cells 24h after plating.

All statistical data were assessed using 2-tailed Student's t-test and are presented as mean±s.e.m. * = $p<0.05$, ** = $p<0.01$, *** = $p<0.001$, **** = $p<0.0001$. Panels B), D)-H) were automatically assessed using ImageJ software. D)-I) were performed double-blinded. Scale bar in A) represents 1mm.

Supplemental Figure 3.

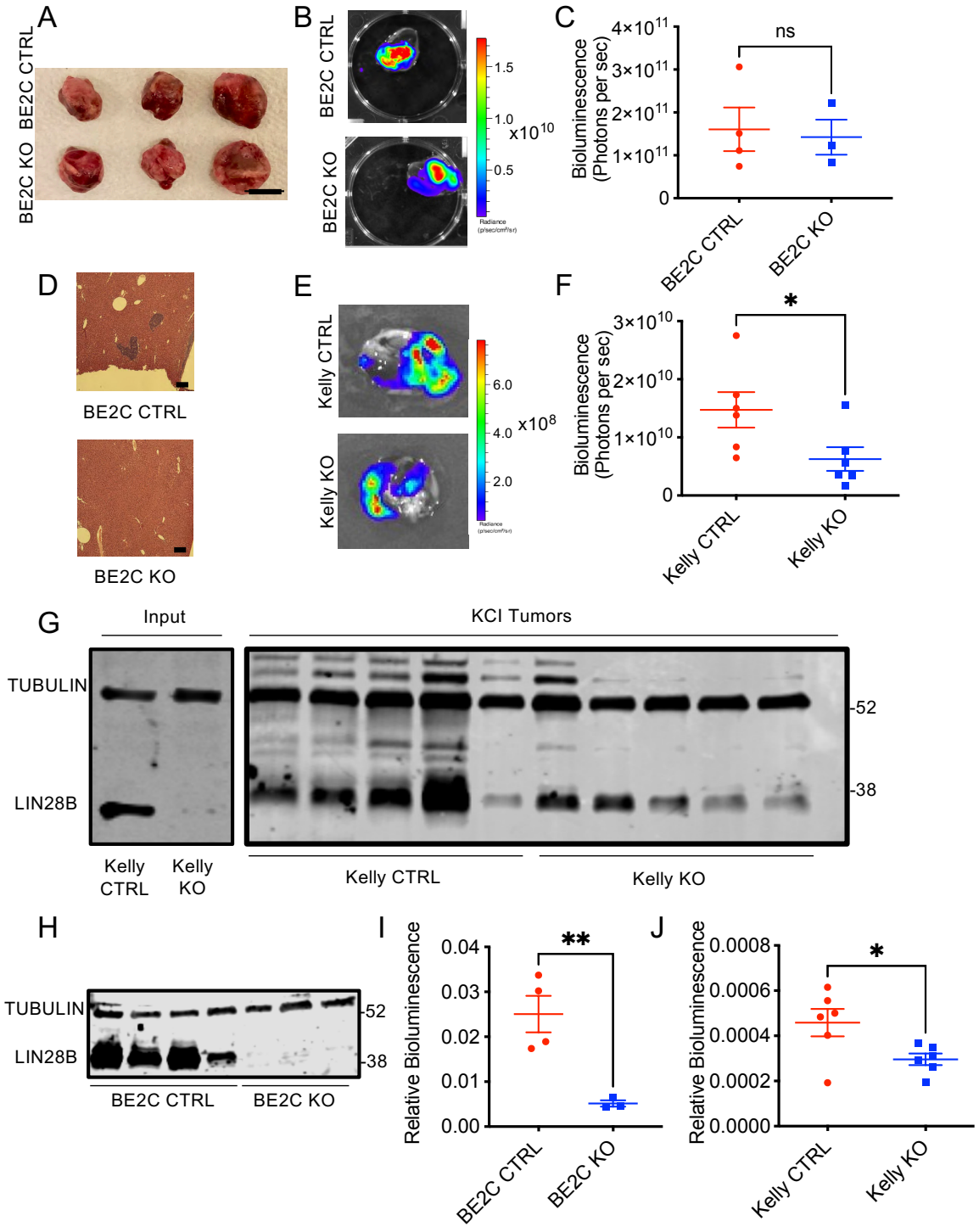

Physical and molecular analysis of primary and metastatic tumors after kidney capsule injection.

A) Representative picture of primary tumors 3 weeks after injection of wildtype (CTRL) and *LIN28B* deficient (KO) BE2C cells under the kidney capsule of NSG mice.
B) Representative bioluminescence images of primary tumors of indicated groups.
C) Graph of bioluminescence of primary tumors of indicated groups used in Figures 2C, 2D (n=4 mice for BE2C CTRL and n=3 mice for BE2C KO).
D) Representative images of histological sections of livers of the indicated groups.

E) Representative bioluminescence images of primary tumors of wildtype (CTRL) and *LIN28B* deficient (KO) Kelly cells injected under the kidney capsule 5 weeks after injection.
F) Bioluminescence analysis of primary tumors of Kelly cells used in Figures 2E, 2F (n=6 mice for Kelly CTRL and n=6 mice for Kelly KO).
G) Western Blot analysis of LIN28B protein expression in Kelly cells (CTRL and *LIN28B* KO) before injection, and in primary tumors 5 weeks after kidney capsule injection (KCI).
H) Western Blot analysis of LIN28B protein expression in BE2C cells (CTRL and *LIN28B* KO*)* of primary tumors 3 weeks after kidney capsule injection (KCI).
I) Relative bioluminescence of livers correlated to the signal of the corresponding primary tumors of mice injected with BE2C cells shown in Figures 2C, 2D.
J) Relative bioluminescence of livers correlated to the signal of the corresponding primary tumors of mice injected with Kelly cells shown in Figures 2E, 2F.

All statistical data were assessed using 2-tailed Student's t-test and are presented as mean±s.e.m. * = $p<0.05$, ** = $p<0.01$. Scale bar in A) represents 1cm. Scale bar in D) represents 200µm.

Supplemental Figure 4.

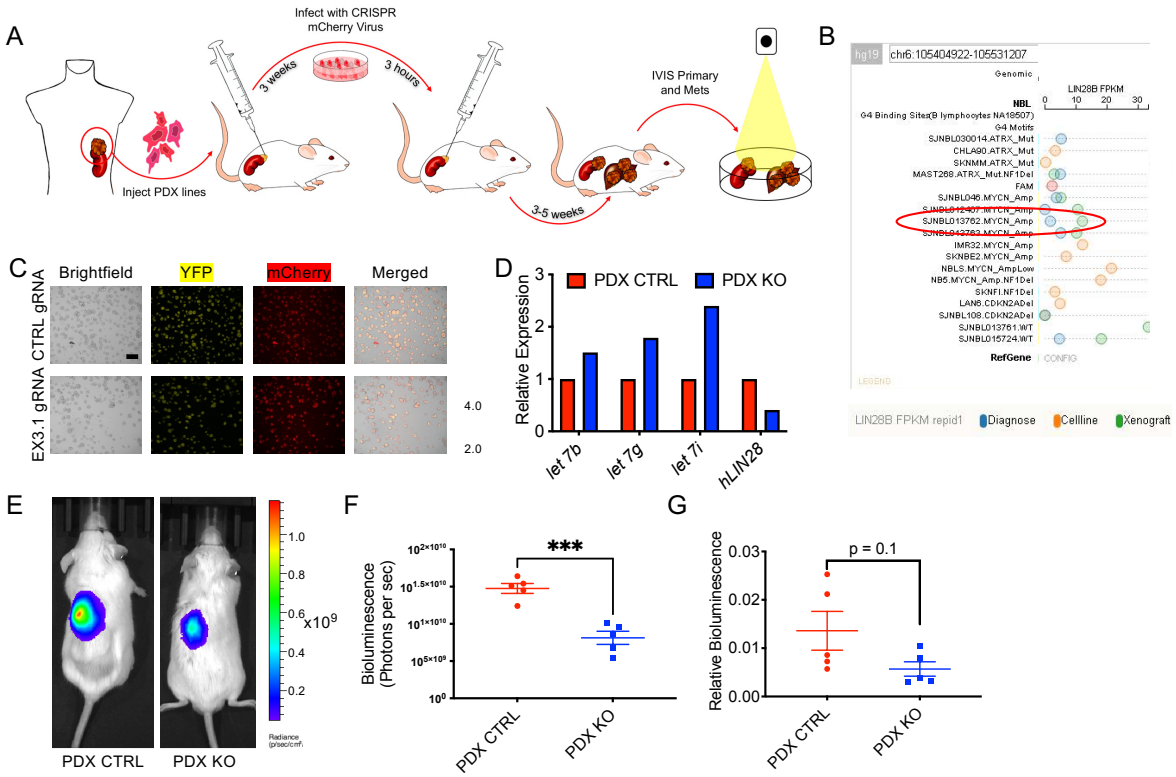

Overview of patient derived xenograft (PDX) experiments.

A) Schematic of experimental design for generating *LIN28B* KO PDX lines, and for evaluating their metastatic behavior.
B) Graph with expression levels of *LIN28B* in the indicated PDX and cell lines.
C) Representative images of yellow fluorescent protein (YFP) expressing PDX spheres 4 days after lentiviral transduction of CRISPR/Cas9 + control gRNA (CTRL gRNA) or EX 3.1 *LIN28B* targeting gRNA (EX3.1 gRNA– *LIN28B* KO), together with the fluorophore mCherry.
D) qPCR analysis of different *let-7* members and *hLIN28B* in the infected PDX lines.
E) Representative bioluminescence image of injected PDX lines 29 days after injection.
F) Quantitative analysis of bioluminescence of mice 29 days after injection of the respective genotypes used in Figures 2G, 2H (n=5 mice/group).
G) Relative Bioluminescence of livers correlated to the signal of the corresponding primary tumor of mice injected with PDX cells shown in Figures 2G, 2H (n=5 mice/group).

All statistical data were assessed using 2-tailed Student's t-test and are presented as mean±s.e.m. * = $p<0.05$, ** = $p<0.01$, *** = $p<0.001$. Scale bar in C) represents 200 µm.

Supplemental Figure 5.

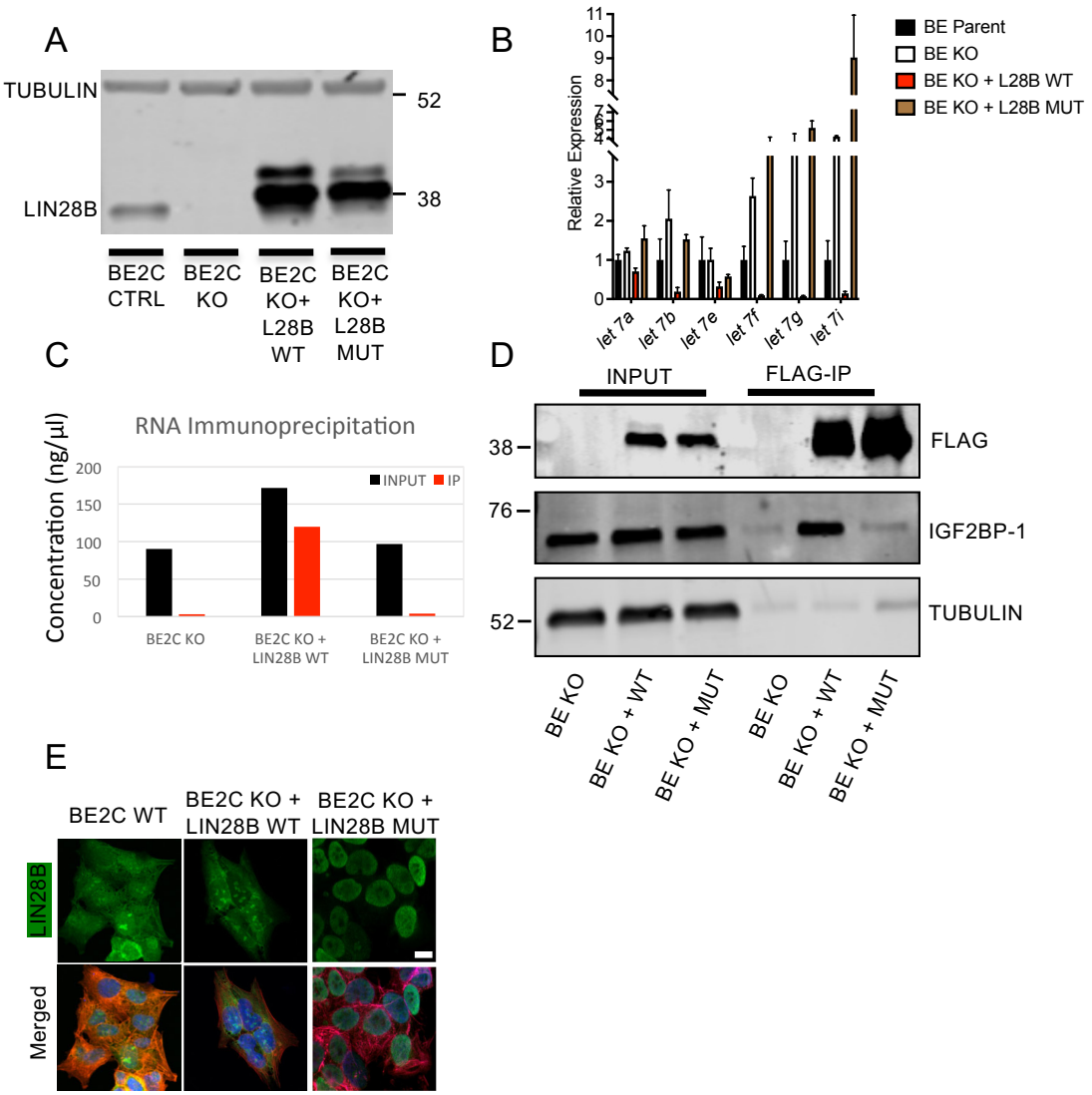

Analysis of BE2C cells lacking endogenous *LIN28B* after re-expression of different LIN28B proteins.

A) Western Blot of BE2C with endogenous LIN28B expression (CTRL), without LIN28B expression (KO), ectopic stable re-expression of either wildtype LIN28B (+LIN28B) or an RNA binding mutant of LIN28B (+LIN28B MUT) in the background of *LIN28B* KO.

B) Relative expression of different *let-7* family members of cells shown in A).

C) Qubit analysis for RNA content after immunoprecipitation of the LIN28B wildtype (WT) and LIN28B RNA binding deficient (MUT) proteins.

D) Western blot analysis of FLAG, IGF2BP-1 and TUBULIN for cells used in C).

E) Representative confocal images of BE2C neuroblastoma cells with either endogenous LIN28B (WT) or exogenous re-expression of LIN28B wildtype (WT) or RNA binding deficient protein (MUT) (Green=LIN28B, Blue=DAPI, Red= F-actin).

Scale bar in E) represents 20µm.

Supplemental Figure 6.

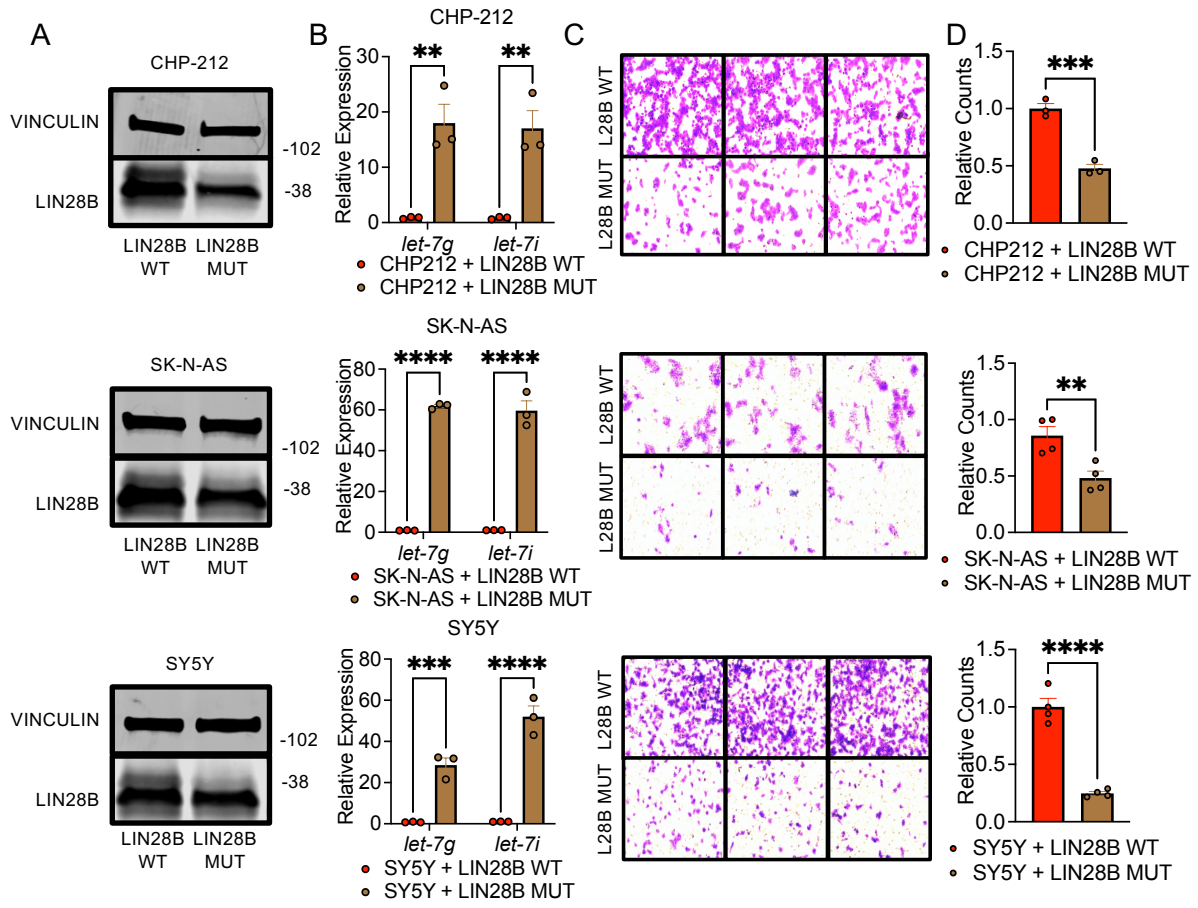

Lentiviral expression of LIN28B WT enhances migratory potential in CHP-212, SK-N-AS and SY5Y cell lines.

A) Western Blot analysis for LIN28B after expression of wildtype (WT) and RNA binding deficient (MUT) LIN28B protein in the indicated cell lines.
B) qPCR analysis of *let-7g* and *let-7i* under LIN28B WT and LIN28B MUT expression.
C) Representative images of transwell migration assays of CHP-212, SK-N-AS and SY5Y cells 24h after plating.
D) Relative counts of migrated CHP-212, SK-N-AS and SY5Y cells 24h after plating (n=3-4 biological replicates/group).

All statistical data were assessed using 2-tailed Student's t-test and are presented as mean±s.e.m. * = $p<0.05$, ** = $p<0.01$, *** = $p<0.001$, **** = $p<0.0001$. Panel D) was automatically assessed using ImageJ software.

Supplemental Figure 7.

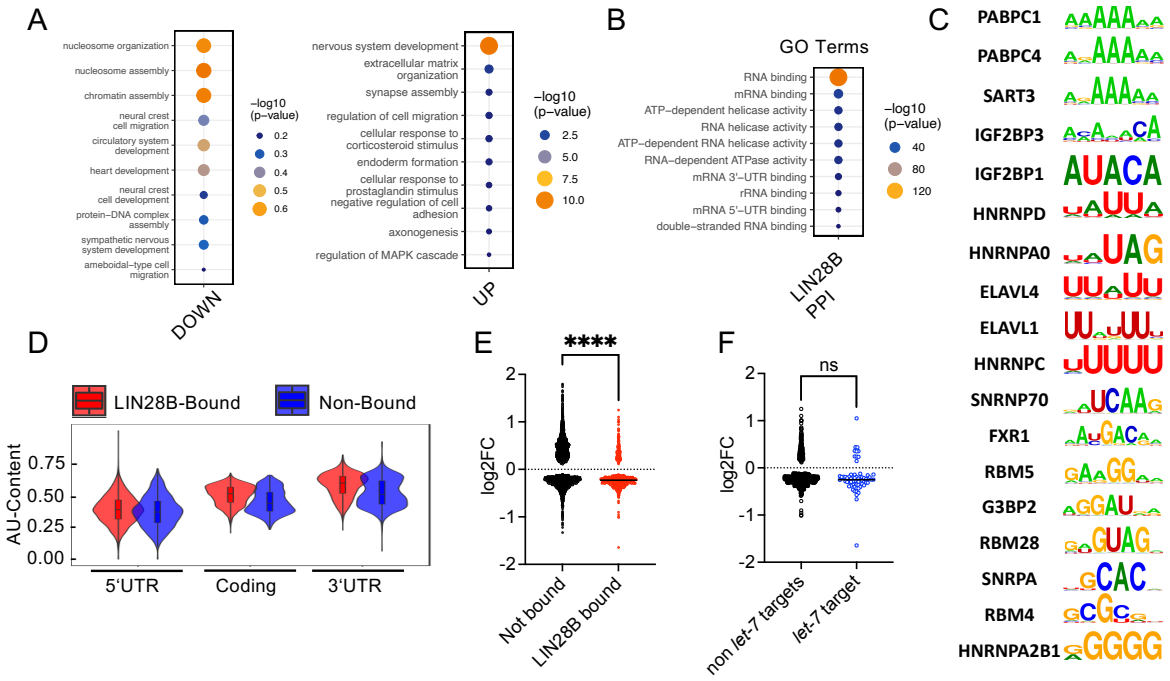

Molecular analysis of datasets for RIPseq, total RNAseq, RNAseq of the polyribosome fraction and LIN28B protein binding partners in BE2C.

A) Gene ontology analysis (GO Biological Process 2018) on significantly up- and down-regulated genes in BE2C *LIN28B* KO.
B) Gene ontology analysis (GO Molecular Function 2018) of LIN28B protein binding partners measured by IP Mass Spec in BE2C.
C) Publicly validated kmer binding motifs of LIN28B protein binding partners.
D) Violin plot depicting AU-content of LIN28B-bound and non-bound transcripts in BE2C CTRL cells.
E) Violin plot of differential expression of LIN28B-bound and non-bound transcripts in total RNA of BE2C neuroblastoma cells in *LIN28B* deficient BE2C compared to LIN28B protein expressing controls.
F) Violin plot for differential expression of LIN28B-bound transcripts depending on their status as conserved *let-7* targets in total RNA of BE2C LIN28B-lacking neuroblastoma cells relative to control.

Differential comparisons in A), E) and F) were made between BE2C *LIN28B* KO vs. BE2C CTRL. Differential comparisons in D) were made between BE2C CTRL vs. BE2C *LIN28B* KO. All statistical data were assessed using 2-tailed Student's t-test, ns = $p>0.05$, * = $p<0.05$, ** = $p<0.01$, *** = $p<0.001$, **** = $p<0.0001$. Gene ontology analyses were performed using Enrichr.

Supplemental Figure 8.

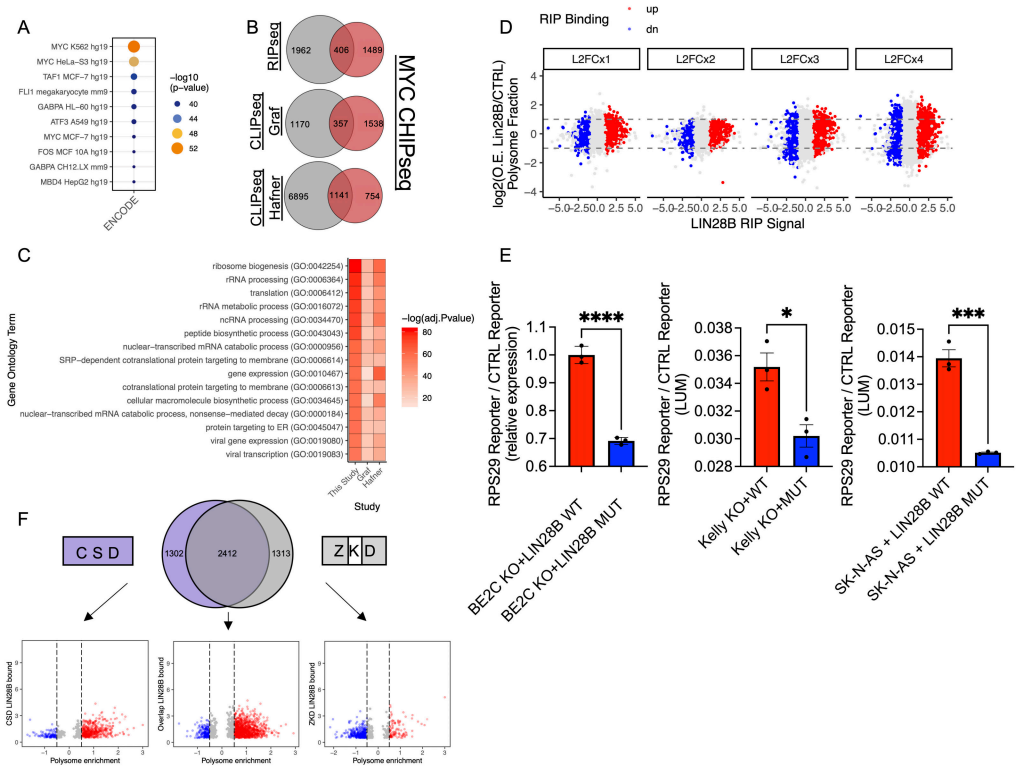

Molecular analysis and comparison of datasets for MYC CHIPseq, LIN28B-RIPseq and CLIPseq as well as RNAseq of the polyribosome fraction of HEK293.

A) Encode TF CHIPseq 2015 enrichment analysis of LIN28B-bound and polysome enriched targets shown in Figure 6A.

B) Venn diagrams depicting the overlap of a MYC CHIPseq dataset in HEK293 and LIN28B RIPseq as well as two LIN28B CLIPseq datasets in HEK293.

C) Gene ontology analysis (GO Biological Process 2018) of overlapped genes in Suppl. Figure 7B.

D) Scatter plot depicting differential expression of the polysome fraction in HEK293 under different LIN28B expression levels (one to four-fold), in relation to LIN28B binding, combining the LIN28B RIPseq dataset with previously published sequencing data of the polysome fraction of HEK293 cells.

E) Bar graphs depicting RPS29-reporter translation by renilla luciferase activity after transfection of the RPS29 reporter plasmid. Activity was normalized to CTRL reporter lacking RPS29 sequence (5' untranslated region, coding sequence and 3' untranslated region).

F) Venn diagram of uniquely bound transcripts of the respective LIN28B binding mutants (intact cold shock domain (CSD) or intact zinc knuckle domain (ZKD)) as well as scatter plots representing the differential polysome enrichment of the indicated groups in BE2C.

Differential comparisons in D) were made between HEK293 LIN28B vs. non expressing. Encode TF CHIPseq 2015 and Gene ontology analyses were performed using Enrichr. Polysome data in D) were derived from (29), CLIPseq data in B) and C) were derived from (26) and (27), MYC CHIPseq data were derived from (36). All statistical data were assessed using 2-tailed Student's t-test and are presented as mean±s.e.m., ns = $p>0.05$, * = $p<0.05$, ** = $p<0.01$, *** = $p<0.001$, **** = $p<0.0001$. Analysis in A) was performed using Enrichr.

Supplemental Figure 9.

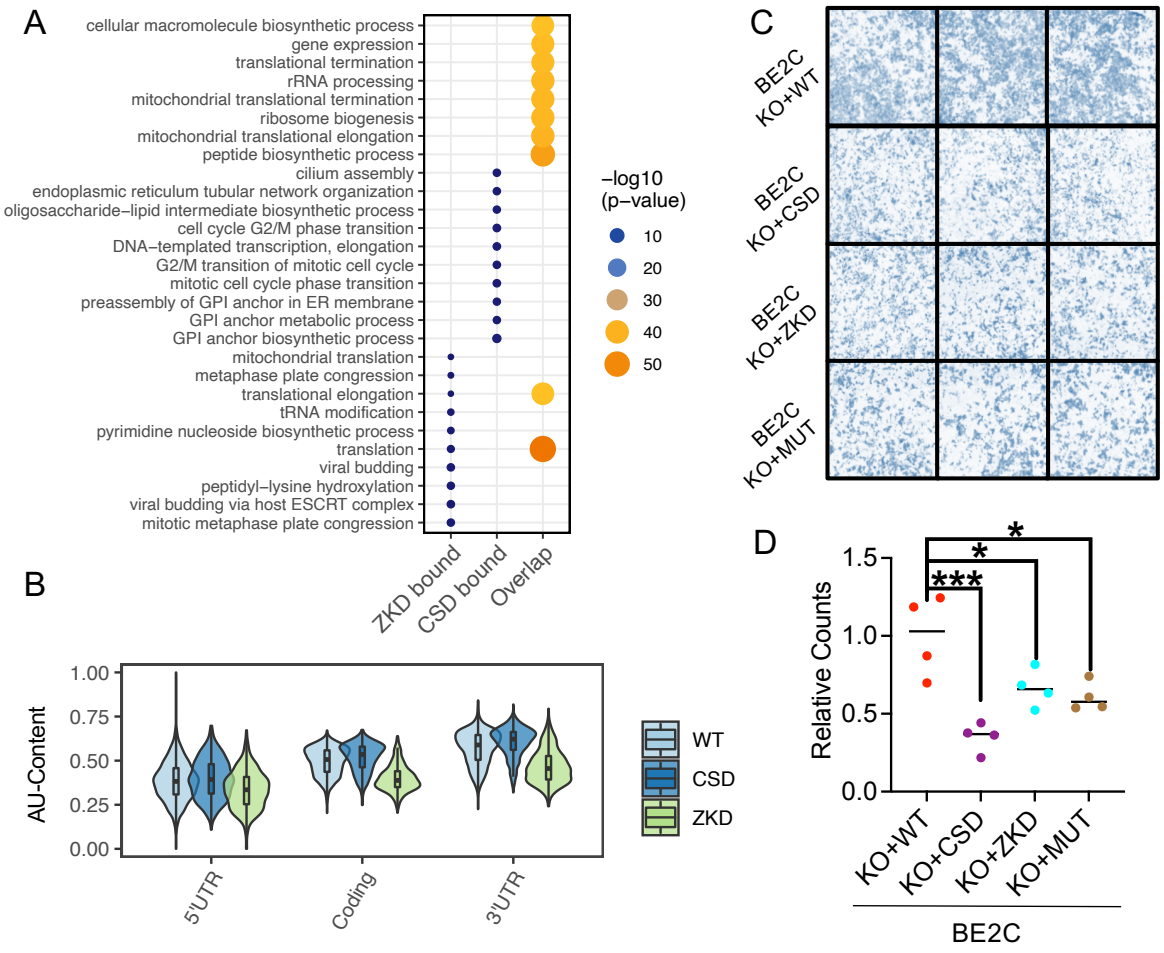

Analysis of the single RNA binding site mutants in BE2C.

A) Gene ontology analysis (GO Biological Process 2018) of transcripts bound uniquely to the zinc knuckle domain (ZKD-bound), uniquely to the cold-shock domain (CSD-bound) or bound by both domains (overlap).

B) Violin plot depicting AU-content of transcripts bound by LIN28B wildtype protein (WT) or uniquely bound by CSD and ZKD, separated for 5' untranslated region (5'UTR), coding sequence (Coding) and 3' untranslated region (3'UTR).

C) Representative images of transwell migration assays of *LIN28B* KO BE2C cells with re-expression of wildtype (KO+WT), CSD binding (KO+CSD), ZKD binding (KO+ZKD) or total RNA binding deficient (KO+MUT) LIN28B protein.

D) Relative counts of migrated BE2C cells used in C) assessed automatically by ImageJ (n=4 biological replicates/group).

All statistical data were assessed using ordinary One-Way ANOVA with Tukey's multiple comparisons test and are presented as mean±s.e.m. * = $p<0.05$, ** = $p<0.01$, *** = $p<0.001$, **** = $p<0.0001$. Gene ontology analyses were performed using Enrichr. Panel C)-D) were performed double-blinded.

Supplemental Figure 10.

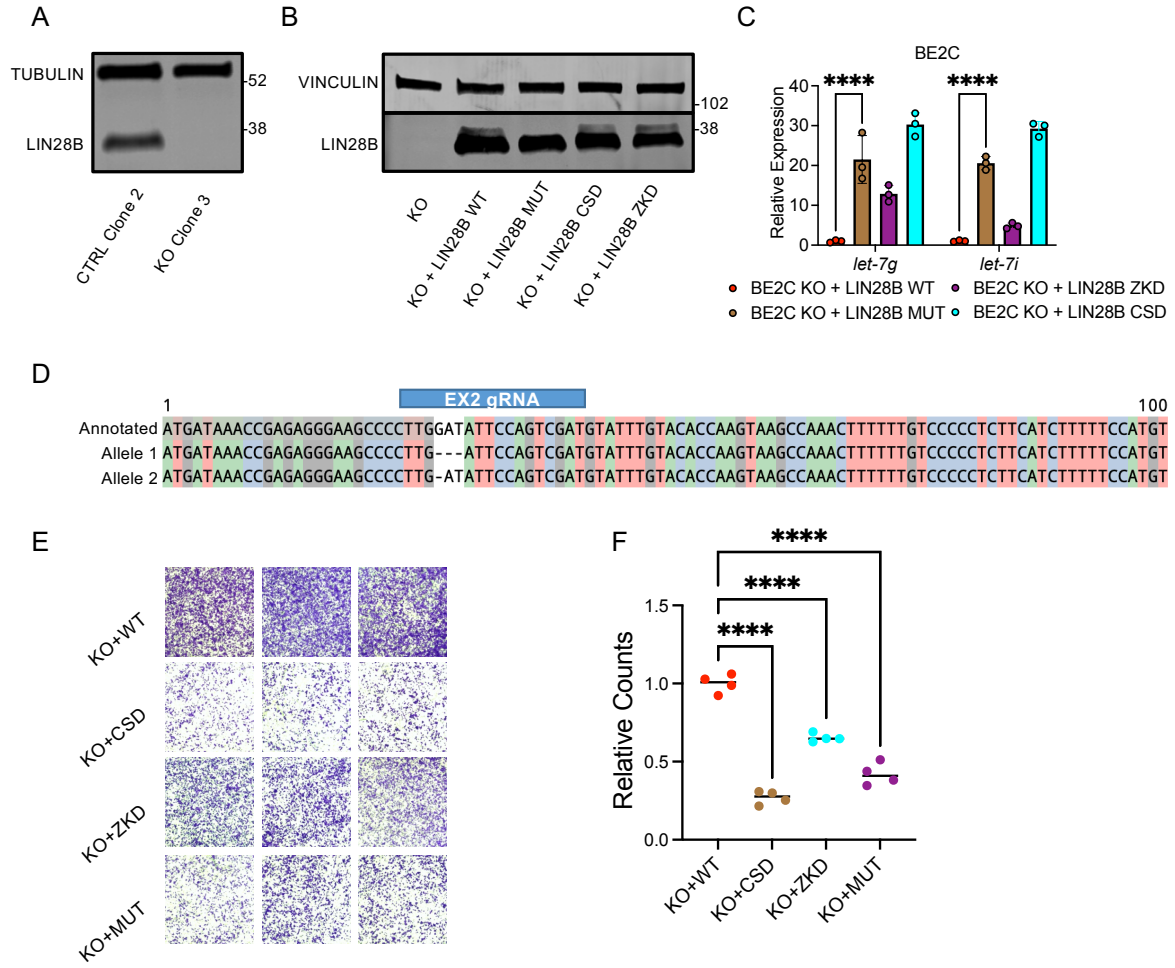

Generation of BE2C *LIN28B* KO clones and repeat of migration experiments.

A) Western Blot analysis of LIN28B in BE2C clones after CRISPR/Cas9 editing using CTRL1 (Clone 2) and *LIN28B* EX2 targeting gRNA (Clone 3).

B) Western Blot analysis of LIN28B of KO Clone 3 before and after lentiviral restoration of LIN28B WT and different RNA binding mutant proteins.

C) qPCR analysis on *let-7g* and *let-7i* after re-expression of different LIN28B proteins shown in B).

D) Confirmation of clonal *LIN28B* KO in BE2C by Sanger Sequencing using CRISP-ID (82).

E) Representative images of transwell migration assays of *LIN28B* KO Clone 3 BE2C cells with re-expression of wildtype (KO+WT), CSD binding- (KO+ZKD), ZKD binding- (KO+CSD) or total RNA binding deficient (KO+MUT) LIN28B protein 24h after plating.

F) Relative counts of migrated BE2C cells used in E) assessed automatically by ImageJ (n=4 biological replicates/group).

All statistical data were assessed using ordinary One-Way ANOVA with Tukey's multiple comparisons test and are presented as mean±s.e.m. * = $p<0.05$, ** = $p<0.01$, *** = $p<0.001$, **** = $p<0.0001$.

Supplemental Figure 11.

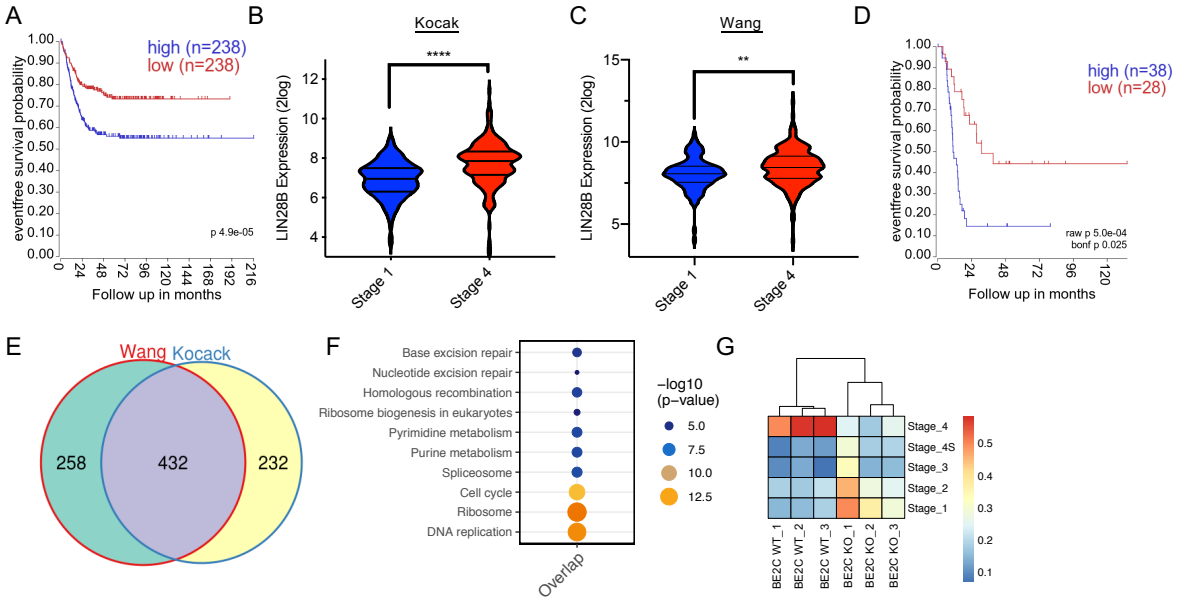

Additional analysis of neuroblastoma datasets.

A) Kaplan Meier Curve of the Kocak neuroblastoma dataset depicting event-free survival for high and low *LIN28B* expressing tumors using median cut-off.
B) Violin plot of *LIN28B* expression in Stage 1 and Stage 4 in the datasets used in Figure 7A).
C) Violin plot of *LIN28B* expression in Stage 1 and Stage 4 in the Wang dataset.
D) Kaplan Meier Curve of the Kocak neuroblastoma dataset depicting event-free survival for high and low *LIN28B* expressing tumors in the *MYCN*-amplified sub-group.
E) Venn diagram depicting the overlap of Stage 4 signature genes of the Wang and Kocak studies.
F) KEGG Analysis of overlapped Stage 4 signature genes.
G) Heat map of the BE2C RNAseq dataset (shown in Figure 4) clustering in the different stages of the Wang study.

Statistical data in B) and C) were assessed using 2-tailed Student's t-test, in A) using log rank test, in D) using Bonferroni correction, and are presented as mean±s.e.m. * = $p<0.05$, ** = $p<0.01$, *** = $p<0.001$, **** = $p<0.0001$. Graphs in A), D) were generated using the R2 database (KaplanScan). KEGG analyses were performed using Enrichr.

Supplemental Figure 12.

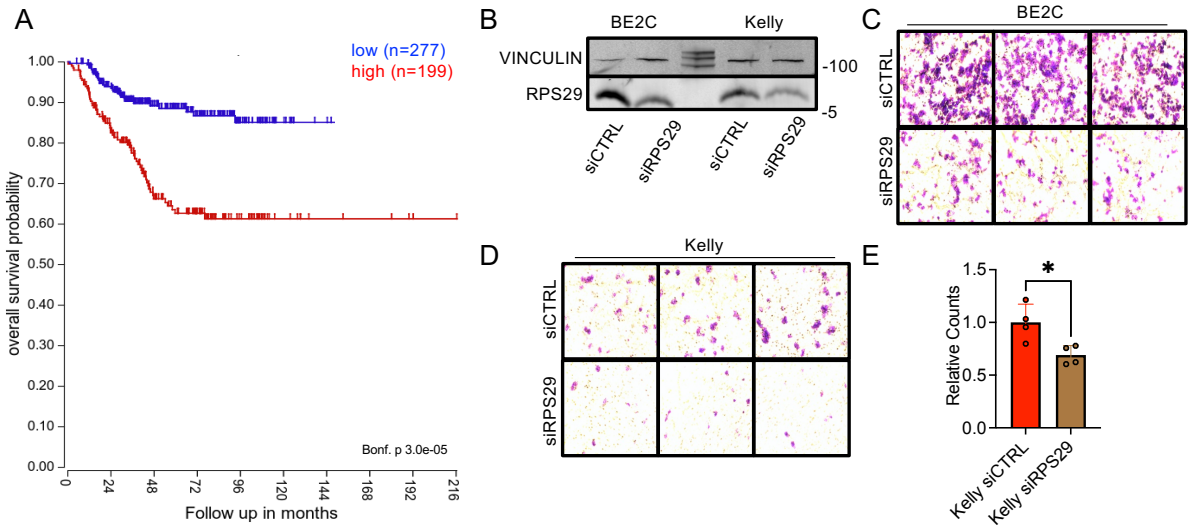

RPS29 is associated with worse survival and loss is diminishing migratory potential.

A) Kaplan Meier Curve of the Kocak neuroblastoma dataset depicting overall survival for high and low *RPS29* expressing tumors using optimal survival cut-off.
B) Western Blot analysis of RPS29 in BE2C and Kelly 72h after transfection of siCTRL and siRPS29.
C) Representative images of transwell migration assays of BE2C cells shown in B) and Figure 7C) 24h after plating.
D) Representative images of transwell migration assays of Kelly cells shown in B) 24h after plating.
E) Relative counts of migrated Kelly cells used in B) and D) assessed automatically by ImageJ (n=4 biological replicates/group).

Statistical data in A) were assessed using Bonferroni correction, in E) using 2-tailed Student's t-test and are presented as mean±s.e.m. * = $p<0.05$.

Supplemental Figure 13.

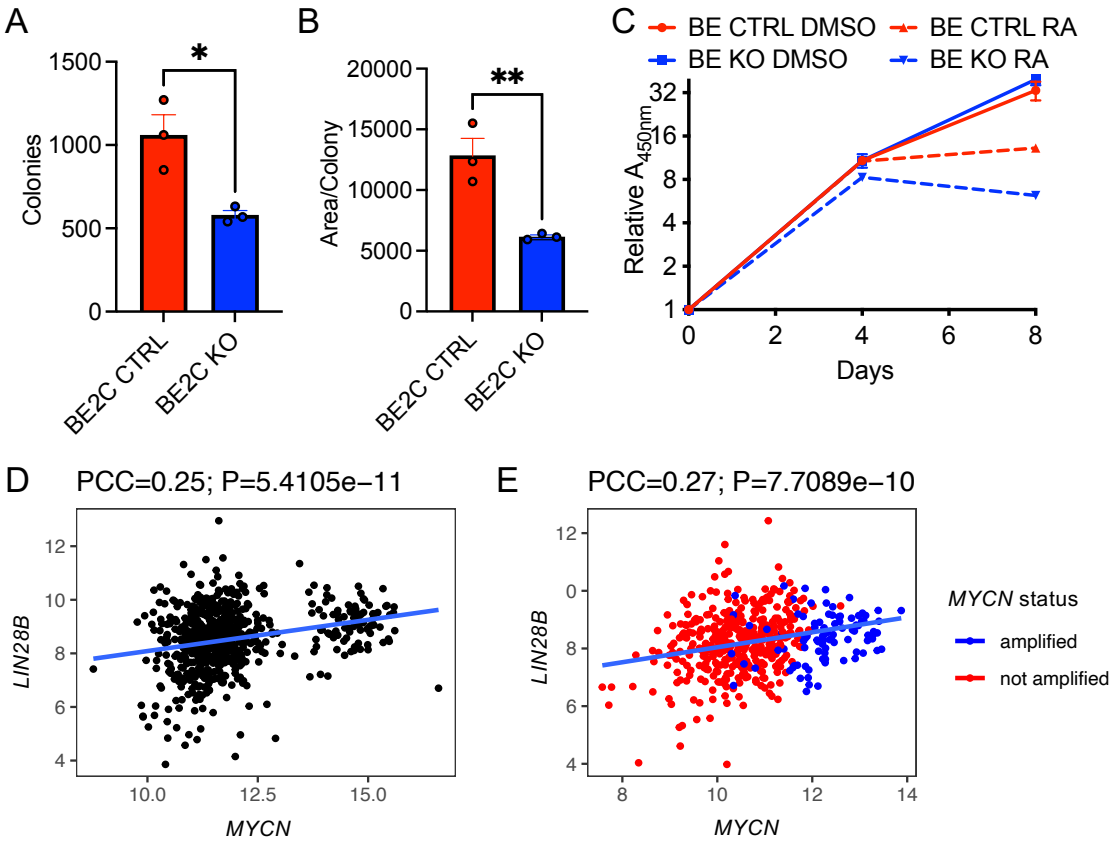

Additional analyses of BE2C after retinoic acid treatment and correlation of *MYCN/LIN28B* mRNA expression.

A) Bar graph depicting the colony number of BE2C CTRL and BE2C *LIN28B* KO Clone 3 after 7 days of 2µM retinoic acid treatment.
B) Bar graph depicting the relative colonized area normalized to the colony number of BE2C CTRL and BE2C *LIN28B* KO Clone 3 after 7 days of 2µM retinoic acid treatment.
C) Cell growth analysis of BE2C CTRL and BE2C *LIN28B* KO treated with either DMSO or retinoic acid.
D) Analysis of the correlation between *LIN28B* and *MYCN* in the Kocak dataset.
E) Analysis of the correlation between *LIN28B* and *MYCN* in the Wang dataset.

All statistical data were assessed using 2-tailed Student's t-test and are presented as mean±s.e.m. * = $p<0.05$, ** = $p<0.01$.

Video 1. Retinoic acid treatment — single wells. Video created from fluorescence images taken daily of GFP-expressing BE2C CTRL and BE2C LIN28B-KO cells treated with 0.6 µM retinoic acid (d0–d10). Final images were composed of 4 separate images to cover a greater area.

Video 2. Retinoic acid treatment — multiple wells. Video created from fluorescence images taken daily of GFP-expressing BE2C CTRL and BE2C LIN28B-KO cells treated with retinoic acid (d0–d9). Each row represents a different concentration of retinoic acid (10, 5, 2, 1.25, and 0.6 µM in DMSO). Final images were composed of 4 separately acquired images to cover a greater area. Because of rare image acquiring errors, some of the smaller images appear black.

Full Blots

Supplemental Figure 1

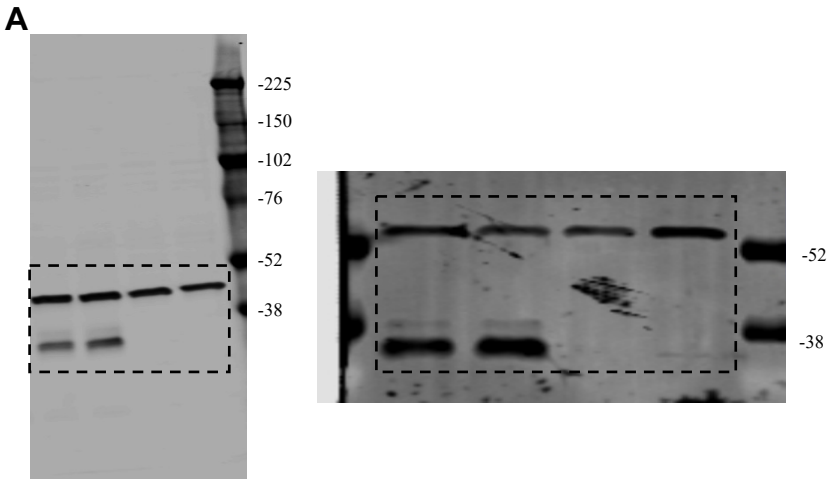

Supplemental Figure 3

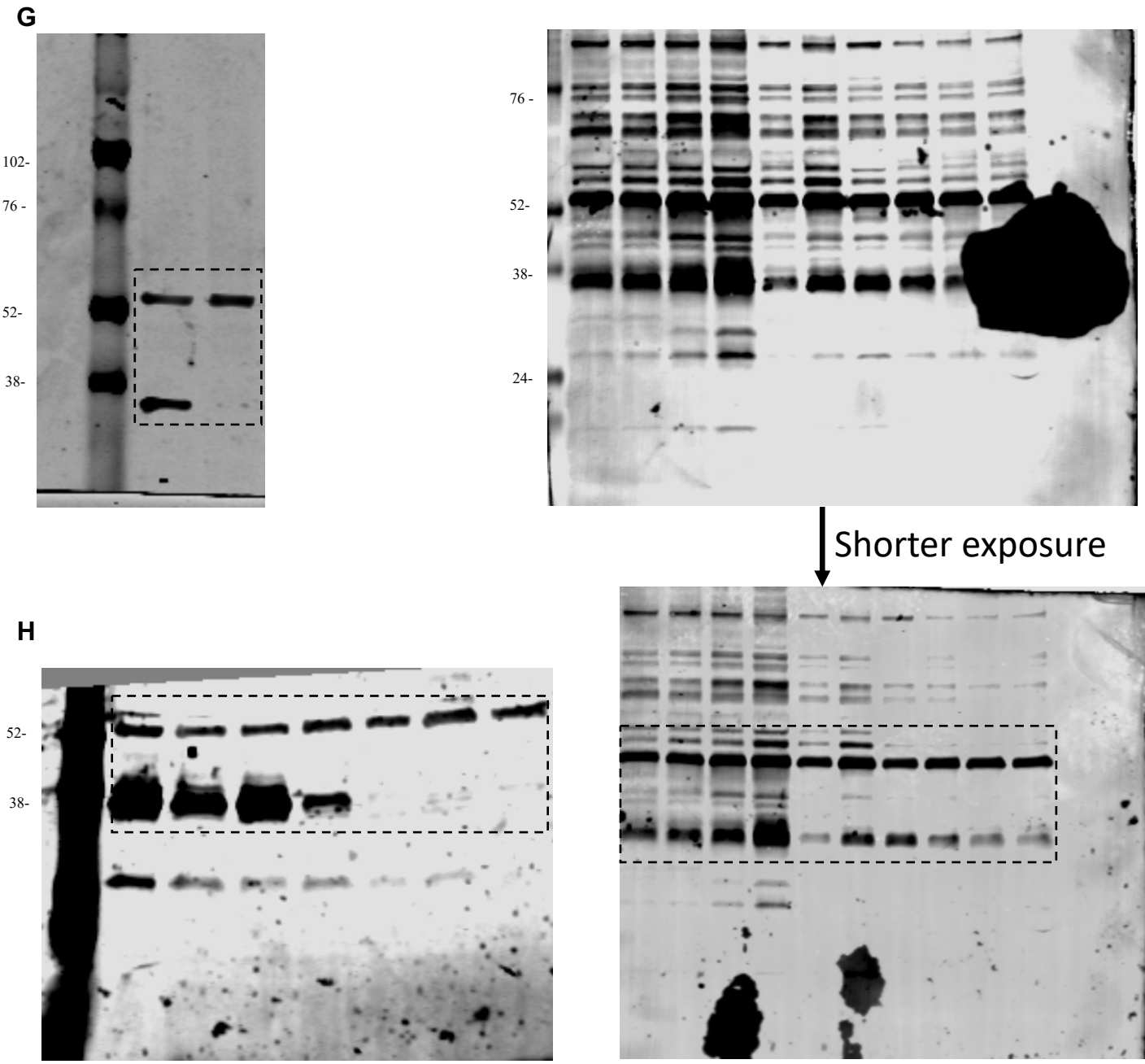

Supplemental Figure 5

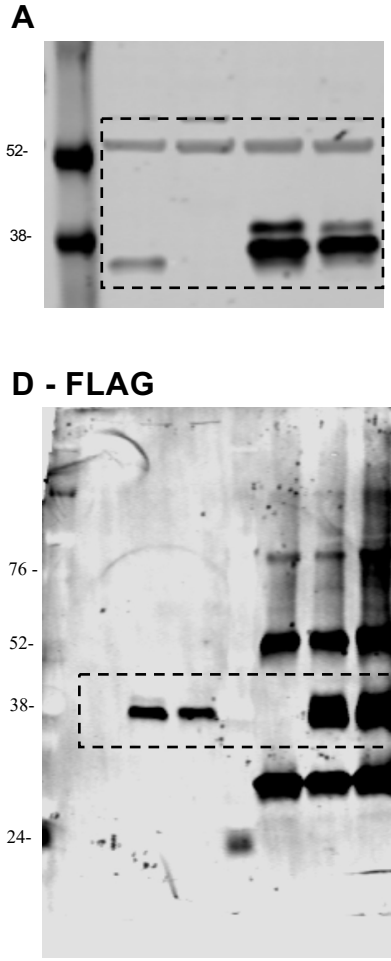

Supplemental Figure 6

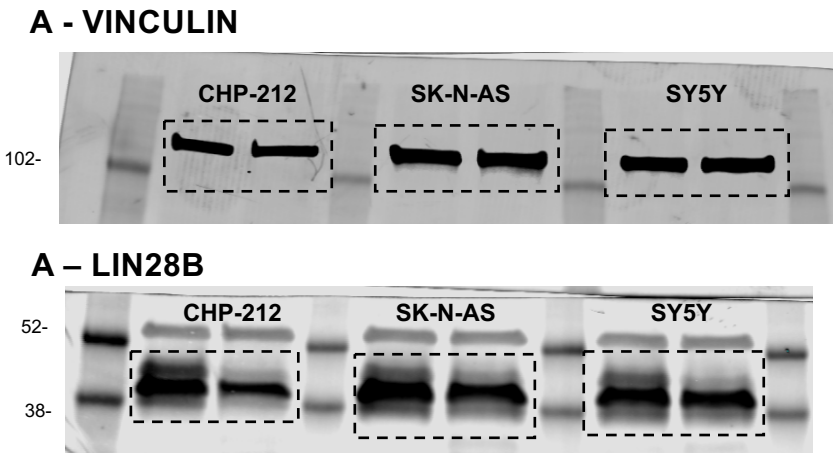

Supplemental Figure 10

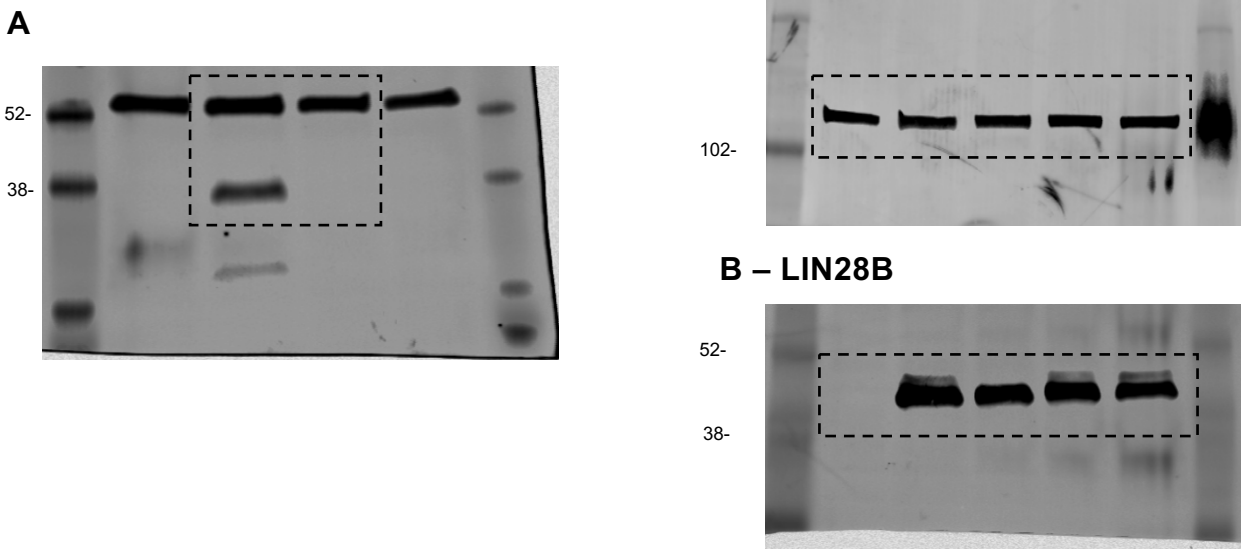

Supplemental Figure 12